Computerised Modelling for Developmental Biology

Bertens, L.M.F.

CHAPTER 6. COMBINING ASPECTS FROM ALGORITHMIC AND EQUATION BASED MODELLING: COMPLEMENTING DIFFERENTIAL EQUATION MODELS OF BIOLOGICAL GRADIENTS WITH PETRI NETS

πάντα ῥεῖ

Everything flows.

- Heraclitus

The final chapter again concerns the formation of biological gradients, modelled using Petri nets. However, a new approach was developed, aimed at quantitative modelling of the process, rather than qualitative. In the current study a merger between aspects of Petri nets and differential equations was strived after, in order to extend the possibilities for simulation and analysis of the net. This has particular merits for computational biology, since quantitative analysis can be performed while still retaining an intuitive understanding of the underlying mechanics of the process.

Manuscript, to be submitted as: Bertens L.M.F., Kleijn J., Hille S., Heiner M., Koutny M., Verbeek F.J., 'Combining differential equation models and Petri net modelling for biological gradient formation'.

6.1 INTRODUCTION

Many biological processes, in particular biochemical processes such as metabolic and signal transduction pathways, have been modelled using differential equations (DEs) (Kicheva *et al.*, 2007; Gregor *et al.*, 2005; Yu *et al.*, 2009; Ellner and Guckenheimer, 2006). These mathematical models accurately describe changes in process variables and thereby enable precise quantitative studies, parameter sensitivity analysis of dynamics and bifurcation analysis. They assume the unfolding of processes in continuous time and even continuous space. This allows the deduction of properties of the system mathematically, *e.g.* the existence and stability of steady states, by analyzing the system of DEs. Analysis is complemented by numerical simulations, to investigate the transient behaviour, when the system is moving towards its long-term behaviour. The simulation techniques involve discretisation of the DEs, in time and space. The resulting computational scheme describes the change of state variables in discrete time steps.

In contrast, algorithmic process models aim to describe the mechanisms underlying the changes in the system (Priami, 2009; Ellner and Guckenheimer, 2006). Petri nets, introduced in the previous chapter, exemplify such a modelling framework (Reisig and Rozenberg, 1998; Petri, 1962; Reisig, 2010). This is of particular use to biological studies, because of its origin in the modelling of chemical reactions and molecular interactions, and its ability to model concurrent behaviour, *i.e.* the potentially simultaneous occurrence of events (*cf.* section 5.2), which is a common feature of biological systems (Fischer *et al.*, 2011; Koch *et al.*, 2011). Moreover, Petri nets combine graphical and mathematical elements, making them intuitive to communicate, execute and understand visually, as we saw for the model of gradient formation in the chapter 5. Implementation of a Petri net yields an operational process model. Using analysis tools such as state space exploration and analysis of *e.g.* deadlocks and boundedness properties, the behaviour of processes can be studied. In this way, they provide a view point complementary to DE models.

As for DE models, an interest in modelling biological processes with Petri nets has emerged, especially in the field of systems biology, and new ways to apply this modelling technique to the life sciences are constantly being developed (Banks, 2009; Gilbert and Heiner, 2006; Gilbert *et al.*, 2007; Chaouiya, 2007; Heiner *et al.*, 2008; Krepska *et al.*, 2008; Matsuno *et al.*, 2003; Steggles *et al.*, 2006; Koch *et al.*, 2011). Petri nets have various advantages for modelling processes in the life sciences. They can be used to model various levels of abstraction in a biological process, ranging from subcellular reactions to processes taking place on tissue or organ level. Key elements, *e.g.* passive resources, active events and concurrency, are found on all these levels, making Petri nets a suitable modelling system. Changing focus from lower to higher levels of abstraction in modelling a biological phenomenon is therefore akin to zooming in and out between levels of magnification. Although, similarly, multi-scale modelling is

feasible with DE-models, as *e.g.* employed in advanced models for weather forecasting, it is more involved to implement, with various numerical mathematical problems to overcome. Additionally, Petri nets can be constructed in a modular fashion, using identical building blocks, for instance to construct groups of similar tissue elements or cells. This makes them easily scalable. Specific elements in Petri net theory, such as Coloured nets, allow one to model several processes taking place simultaneously at the same location.

Aim of the study

In this chapter we present our work on combining Petri nets with differential equation models, in order to construct a generic Petri net model for the formation of molecular gradients. In chapter 5 a model has been presented, where the process of gradient formation is modelled as a global decrease in concentration levels of molecules throughout the cells in the tissue, and in which the spread of molecules is governed by a fixed ratio ρ of molecular concentration between neighbouring cells (*cf.* section 5.3.3). This ratio represents the combined effect of molecule transport and degradation in the cells.

In the current chapter we present an elaboration of this earlier model to include parameters of DE modelling. In this way, we continue the investigation of the use of Petri nets for the field of higher level developmental biology. The model presented in chapter 5 can be seen as a proof of concept, in which the modelling method was tested out in an abstract manner, allowing us to thoroughly check the correctness of the underlying assumptions (in particular token preservation, monotonicity, ratio and termination, *cf.* 5.4.1). The model presented in the current chapter builds on this proof of concept and moves from an abstract approach, towards a more detailed and applied approach. Here, the events of molecule production, diffusion and degradation have been modelled explicitly and are governed by individual parameters.

For the process of gradient formation, DE models exist which provide accurate quantitative data about the gradient formation (Kicheva *et al.* 2007; Gregor *et al.*, 2005; Yu *et al.*, 2009). By linking the parameters of the Petri net model to the parameters in the discretised form of such a DE model, the net can be used to produce quantitative data about discrete space and time points in the process, similar to the DE model, while at the same time retaining the advantages of the Petri net framework. In order to validate the Petri net model, we present a case study; from literature we have selected a study in which experimental observations of gradient formation have been modeled using differential equations. We use the parameters from this DE model and show how the execution data from the resulting Petri net correspond to the data obtained from the differential equations.

Since this study forms a continuation of the study presented in chapter 5 the reader is referred to sections 5.2. and 5.3 for Petri net terminology and definitions, the biological background of gradient formation and the modelling decisions. In the remainder of this chapter the discretisation of the DE model is set out, along with the connection of DE parameters to parameters in the Petri net modelling solution, in section 6.2. In 6.3 we present the resulting Petri net model. A case study of gradient formation of the protein Dpp in the fruit fly is used for the validation and presented in section 6.4; finally, conclusions and remarks on future work can be found in section 6.5.

6.2 DERIVATION OF PETRI NET MODEL PARAMETERS FROM A DISCRETISED DE MODEL

In this section the temporally and spatially continuous situation, modelled by a DE model, is translated to a discrete situation, which is subsequently linked to the Petri net solution, described in section 6.3. We consider the following reaction-diffusion equation

$$\frac{\partial C}{\partial t} = D\frac{\partial^2 c}{\partial r^2} - kC\,, \tag{1}$$

on the one-dimensional interval (0, L). This is used in (Kicheva *et al.*, 2007) as the effective equation to describe their data. It consists of the measurement of fluorescence of GFP-labelled morphogens when these form a gradient in a rectangular sample of cell tissue. The morphogens are homogeneously emanating from a source, which is a strip of cells at the left border (r = 0) of this rectangle. The morphogens move from the source to the right, *i.e.* towards $r = L$. The fluorescence measurements are made in multiple vertical layers in the tissue and summed, reducing the situation to two dimensions. The morphogen concentration can be assumed constant in the direction transversal to r, further reducing the situation to one dimension. Thus, $C(r,t)$ represents the areal density of observed morphogen at location r at time t (in molecules/μm^2). D is the effective diffusion coefficient ($\mu m^2/s$), combining passive diffusion and possible other transport processes such as endocytosis and active diffusion (*cf.* section 5.3.1), and k is the degradation rate (s^{-1}). Equation (1) is complemented with an initial condition $C(r,0) = f(r)$ and zero-flux boundary conditions at L and constant influx areal density J_0 through the left side of the sample at r = 0, *i.e.* $D\frac{\partial}{\partial r}C(0) + J_0 = 0$.

The standard procedure of spatial discretisation at equidistant points $0 = r_0 < r_1 < \cdots < r_n = L$, with $l = r_{i+1} - r_i$ and $C_i(t) := C(r_i,t)$, followed by temporal discretisation at time points t_j, in which j represents the number of steps and the steps are equally separated at time intervals Δt (corresponding to a fixed number of n' steps); this yields

$$\frac{\Delta C_i(t_i)}{\Delta t} \approx \frac{D}{l^2}(C_{i-1}(t_j) - 2C_i(t_j) + C_{i+1}(t_j)) - kC_i(t_j) \quad (2)$$

for i = 1, ... , n - 1, where $\Delta C_i(t_j) := C_i(t_{j+1}) - C_i(t_j)$. We take l equal to the cell length and h to the cell height. Multiplying both sides of (2) with the cell area $A = l\,h$ in the plane of observation yields a similar, slightly rewritten expression for the change in the number $m_i = m_i(t_j)$ of molecules in cell i at

time t_j (omitting time dependence):

$$\Delta m_i \approx \frac{D\Delta t}{l^2}(m_{i-1} - m_i) - \frac{D\Delta t}{l^2}(m_i - m_{i+1}) - km_i\Delta t \quad (3)$$

for i = 1, ... , n - 1, with $\Delta m_i = m_i(t_{j+1}) - m_i(t_j)$. Approximation (3) is appropriate when Δt and l are such that $D\Delta t/l^2 < 1$ and $k\Delta t < 1$ are sufficiently small. Equation (3) is complemented by similar equations at i = 0 and $i = n$ that incorporate the boundary conditions:

$$\Delta m_0 = J_0 h\Delta t - \frac{D\Delta t}{l^2}(m_0 - m_1) - k\Delta t m_0 \quad (4)$$

$$\Delta m_n = \frac{D\Delta t}{l^2}(m_{n-1} - m_n) - k\Delta t m_n \quad (5)$$

In order to arrive at a Petri net model which incorporates these derivations, we use the abstract Petri net presented in chapter 5 and specify this to include the derived parameters. We start with a Petri net with a *max-enabled* semantics and places x_1, ... , x_n which represent biological cells (as described in chapter 5). We then extend this with specifications of the three main events in the process of gradient formation, using the given derivations:

I) the first term on the right hand side of (4) represents morphogen **production** in the source and transport to the first cell, x_1 (note that the token preservation from the earlier model no longer applies, *cf.* 5.4.1).

II) the **transport** between neighbouring cells x_i and x_{i+1} is given by the first two terms on the right hand side of (3).

III) lastly, the **degradation** in every x_i is given by the third term on the right hand side of (3).

In other words, the marking of the places x_i (for all places except x_1) after a multiple j of n' steps (in which n' represents one cycle of the modeled process, *cf.* 5.4.2) can be approximated well by the solution of the diffusion equation (1) at times $t_j = j\Delta t$:

$$m_i(jn') \approx h\int_{(i-1)l}^{il} C(r,t_j)dr \approx lh \cdot \frac{1}{2}\left[C((i-1)l,t_j) + C(il,t_j)\right] \qquad (6)$$

where we have used the trapezium rule to approximate the integral. In this way we aim to relate the number of molecules m_i to the marking of place x_i, *i.e.* $m(x_i)$. This brings us to the Petri net solution and its exact workings.

6.3 MODELLING SOLUTION

The previous section illustrated the derivation of parameters from the DE model, for the elements production, transport and degradation. In this section we present in detail our Petri net model and describe its workings. We propose a formal, general Petri net model for gradient formation. Given is a segment of n adjacent biological cells with the i-th cell the immediate neighbour of the (i+1)-th cell. This is represented in the Petri net by x_1, ..., x_n places. Morphogens are represented by tokens and can be transported only between immediate neighbours. Transitions t'_1, ..., t'_n represent the transport of tokens, in the direction x_1 to x_n. We will focus on one-directional gradient formation, strictly from x_1 to x_n. Figure 6.1A shows the basic structure of the net; here the first neighbouring cells on the left side of the modelled biological tissue are shown, x_1, x_2 and x_3.

In section 6.2 we discussed the derivation of parameters from differential equations for three basic elements in the process. Here we explain the way in which these parameters have been incorporated into the Petri net model.

I) Morphogen **production** and transport from the source to the adjacent cell x_1 are modelled by the transition s and comply to the first term of (4), which is directly translated to the weight arc of s to x_1. The weight is therefore $J_0 h\Delta t$.

II) With the exception of x_1 and x_n the morphogen **transport** from x_i to x_{i+1} follows the first term on the right hand side of (3), which corresponds to the effective diffusion from left to right. In order to incorporate this term into the weight arcs of the Petri net and therefore determine the number of tokens to be transported from x_1 to its neighbour x_{i+1}, additional auxiliary places are used for all $1 \le i \le n$: x'_1, ... , x'_n and x''_1, ..., x''_n. These places are initially empty. The places x'_i and x''_i are filled with $pD\Delta t \cdot m_{x_i}$ tokens and place x'_{i+1} and x''_{i+1} are filled with $pD\Delta t \cdot m_{x_{i+1}}$ tokens. After this first step in which

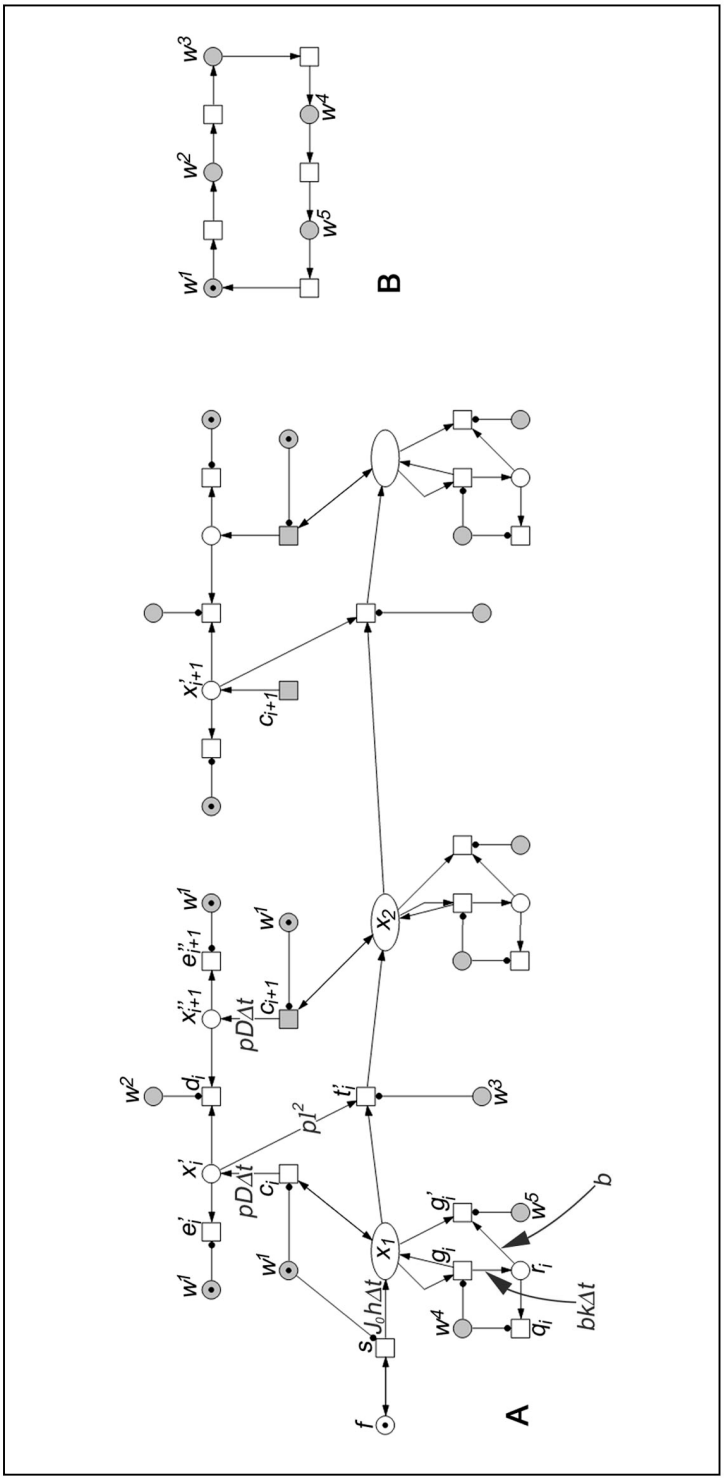

Figure 6.1. The main construction of the net, shown for three neighbouring cells (A) including production of morphogens (transition *s*) and influx of these in the first cell (x_1); the auxiliary net in (B) determines the order of events in the main net. Note that grey places are fusion places.

places x'_i and x''_{i+1} are filled, these places get depleted simultaneously up to the point where x''_{i+1} is empty, leaving x'_i with a token difference of $pD\Delta t \cdot m_{x_i} - pD\Delta t \cdot m_{x_{i+1}}$. The number of tokens to be transported from x_i to x_{i+1} is $\beta_i = \frac{pD\Delta t \cdot m_{x_i} - pD\Delta t \cdot m_{x_{i+1}}}{pl^2}$.

In other words, for every pl^2 tokens in place x'_i a token is moved by transition t'_i from x_i to x_{i+1}, respectively. Note that the multiplication by p in the previous step is countered here by a division in which the token number is rounded off; this multiplication constant is added to limit deviations caused by rounding off (*cf.* 6.4). Apart from multiplication with and division by p, the steps described here correspond directly to the derivation in (3) without the element of degradation (discussed below), as can be seen from the following:

$$m'_{x_i} = m_{x_i} - \beta_i + \beta_{i-1} = m_{x_i} - \frac{pD\Delta t \cdot m_{x_i} - pD\Delta t \cdot m_{x_{i+1}}}{pl^2} + \frac{pD\Delta t \cdot m_{x_{i-1}} - pD\Delta t \cdot m_{x_i}}{pl^2} \quad (7)$$

$$m'_{x_i} = m_{x_i} - \frac{D\Delta t}{l^2}(m_{x_i} - m_{x_{i+1}}) + \frac{D\Delta t}{l^2}(m_{x_{i-1}} - m_{x_i}) \quad (8)$$

Note that the monotonicity, described for the net in chapter 5, is maintained in the transport of this net. When no degradation takes place, monotonicity holds in the same way as described in 5.4.2.

III) Simultaneously with morphogen transport, morphogen **degradation** also takes place in the cells, which corresponds to the third term on the right hand side in (3). For every x_i, this process is modelled by the transitions g_i and g'_i and the place r_i, which is again an auxiliary place used to determine the number of tokens to be removed from x_i. The place r_i is filled with $bk\Delta t$ tokens (multiplication with b is used to prevent having to round off $k\Delta t$, since due to the small value of k for most biological gradients, this will often lead to 0) and subsequently for each amount of b tokens in r_i a token from x_i is removed, *i.e.* degraded. This results in a degradation element $\frac{bk\Delta t}{b} = k\Delta t$, which corresponds with the third element on the right hand side in (3). When k is identical for all x_i, monotonicity is still ensured (as in the case study discussed in 6.4).

These processes of production, transport and degradation take place in a cycle of $n' = 5$ steps. Note that n' was used in 6.2 to obtain the number of steps by multiplying this with the number of cycles, j; thus, in the translation from DE to Petri net parameters, $\Delta t = n'j$. An auxiliary net, shown in Figure 6.1B, is used to regulate these phases and the corresponding transitions. This auxilliary net is similar to the one presented in chapter 5; there, degradation was not modelled in explicit steps (diffusion

and degradation were combined in one parameter) and the cycle was limited to $n' = 3$ steps.

As described in 5.4.2, the auxiliary net controls the transitions via n' places, in this case w^1 to w^5, and activator arcs. For the full picture of the system one should combine a single copy of the auxiliary net to the figures for all of the pairs x_i, x_{i+1}. For clarity's sake the auxiliary net is only drawn once and places with identical labels should be identified as one place (in Fig. 6.1 and 6.3 fusion places are shown in grey). In the auxiliary net a token moves from one place to the next for each step in the cycle and the events in the main net are scheduled by these token movements in the following order, in which the number of the steps corresponds to the number of the place w which contains a token at that point:

1. For $1 \le i \le n$, transition c_i fills (in m_{x_i} auto-concurrent occurrences) place x'_i with $pD\Delta t \cdot m_{x_i}$ tokens and transition c_{i+1} fills (in $m_{x_{i+1}}$ auto-concurrent occurrences) place x''_{i+1} (and simultaneously x'_{i+1}) with $pD\Delta t \cdot m_{x_{i+1}}$ tokens. In the same step transitions e'_i and e''_{i+1} empty x'_i and x''_{i+1} of any residual tokens left from the previous cycle. In addition, if place f contains a token, transition s outputs $J_0 \cdot \Delta t \cdot h$ morphogens to x_1.

2. Transition d_i removes tokens from places x'_i and x''_{i+1} in $m_{x''_{i+1}}$ auto-concurrent occurrences, thereby emptying x''_{i+1} and leaving the difference in x'_i ; in other words, $m_{x'_i} = pD\Delta t \cdot m_{x_i} - pD\Delta t \cdot m_{x_{i+1}}$ in.

3. Transition t'_i fires and transports $\alpha/100l^2$ tokens from x_i to x_{i+1}.

4. In step 4 and 5, the degradation of morphogens in the individual cells is addressed. In this step transition g_i inserts $bk\Delta t \cdot m(x_i)$ tokens into place r_i. Simultaneously, transition q_i empties r_i of any residual tokens left from the previous cycle.

5. Subsequently, transition g'_i removes one token from x_i for each b tokens in r_i.

Due to the auxiliary net, neighbouring pairs of cells are either all involved in calculation steps (steps 1, 2 and 4) or tokens are transferred between or removed from cells. During the calculation steps the token numbers in all places x_i, representing the biological cells, except place x_1 are therefore unchanged and can be accessed for reading by other transitions. In other words calculations are *orthogonal* to the basic operations of gradient formation. Another important feature of this approach is that it is purely local; interactions between neighbouring cells are independent of the token numbers in other cells or the length of the chain of cells.

6.4 A CASE STUDY OF DPP GRADIENT FORMATION TO VALIDATE THE PETRI NET MODEL

For a validation of the Petri net model we use data from (Kicheva *et al.*, 2007). In this study, gradient formation was examined for the protein Dpp (Decapentaplegic), in the wing of the fruit fly, *Drosophila melanogaster*. These proteins were studied as they emanated from a source through the wing epithelium. The gradient could be treated as a series of places. The 3D situation was captured in a stack of images. Firstly, a maximum projection of this stack reduced the tissue to a two-dimensional plane; this could further be reduced to a line of places, since the rectangular region of interest lay parallel to the rectangular source tissue and movement at the lateral sides was negligible *cf.* section 6.2.

Kicheva *et al.* (2007) studied the behaviour of gradient formation and the role played in this by the process of endocytosis, *i.e.* the uptake of particles through membrane vesicles into the cell (*cf.* section 5.3.1), which is known to contribute to the formation of many gradients, in addition to diffusion (Fischer *et al.*, 2011; Gurdon and Bourrillot, 2001; Lander *et al.*, 2002; Scholpp and Brand, 2004; Teleman *et al.*, 2001). To this end the authors created a partial endocytotic block in animals which were mutant for the *shibire* allele and in which the source was rescued by a *shibire*$^{+}$ transgene. Using an experimental setup, monitoring fluorescent recovery after photobleaching (known as a FRAP assay), the values for D and k were determined under different experimental conditions of the gradient formation. Here we simulate the process for the *Dpp shibire* mutant at 32°C (Dpp-rescue) and the Dpp control group at 32°C (Dpp).

For these conditions the following values for D and k were found by Kicheva *et al.* (2007) and used in the Petri net model presented here (omitting the standard deviation): for Dpp $D = 0.10$ and $k = 2.52$ and for Dpp-rescue $D = 0.06$ and $k = 1.53$. Based on these values, values for p and b were set at $p = 10^2$ and $b = 10^5$, in order to minimize errors in rounding off. The simulation results from the Petri net model are compared to those predicted by the DE model (1), using the experimentally determined parameter values for D, k, l, j_0 and h as found by Kicheva *et al.* (2007). For this validation the number of cells to be modelled has been set at 30, which is a large enough number to accurately model L, given the current case study. The Petri net therefore describes the situation of a linear array of 30 cells, with a constant influx of morphogen at the left ($r = 0$). At the far right side we assumed that morphogens cannot flow out of the last cell. In our DE model this is represented by zero flux boundary conditions at $r = L$ (see section 6.2; $L = 30l$). Note that this differs from the DE model employed in Kicheva *et al.* (2007), where the array of cells is assumed to extend infinitely far. The finite number of cells in the Petri net has been taken into account in the derivation of parameters from the differential equations (*cf.* 6.2).

Gradient formation is considered finished once a steady state has been reached, *i.e.* a state in which morphogen concentrations stay the same in all cells, due to a balance between production, diffusion and degradation. For the diffusion equation model, the exact steady-state solution *C** to the diffusion equation (1) is given by

$$C^*(r) = \frac{j_0}{\sqrt{kD}} e^{-\mu r}, \qquad \mu := \sqrt{k/D} \tag{7}$$

In our case, with a finite array of cells and Neumann conditions at $r = L$, (7) requires an additional correction factor: the exact steady state solution becomes

$$C^*(r) = \frac{j_0}{\sqrt{kD}} e^{-\mu r} \cdot \frac{1 + e^{2\mu(x-L)}}{1 - e^{-2\mu L}} \tag{8}$$

For comparison of the density description by means of *C* with the number of tokens in a cell as computed by the Petri net the first must be converted to the number N_k of morphogen molecules in cell k, by means of

$$N_k(t) := h \int_{(k-1)l}^{kl} C(r,t)\,dr, \tag{9}$$

where l denotes the cell length, *h* the cell height and *k* = 1, 2, ... , 30. The integral in (9) is approximated by means of the basic trapezoidal rule, yielding

$$N_k(t) \approx hl \cdot \frac{1}{2}\big[C((k-1)l,t) + C(kl,t)\big]. \tag{10}$$

Here l = 2,6 μm and *h* = 2,6 μm.

In the Petri net a steady state is reached once the marking of the entire net stays identical for two consecutive step cycles, since the behaviour of the net is deterministic and the parameter values remain unchanged. For each of the experiments the Petri net solution with corresponding parameter values was implemented in the software tool Snoopy (Rohr *et al.*, 2010) and markings of the places $x_1, \ldots, x_n$ for every 5 steps were obtained using our in-house analysis tool PetriCalc. Snoopy was used as an interface for the creation of the net, but due to the size of the net and the high numbers of tokens to be processed, analysis was done with PetriCalc. This has been developed based on the analytical methods of Snoopy. The steady state, as reached by the Petri net for Dpp and Dpp-rescue, was found to closely correspond to the steady state given by (8) and (10), with only minor deviations: at most 1.4 % for Dpp-rescue and 0.2 % for Dpp.

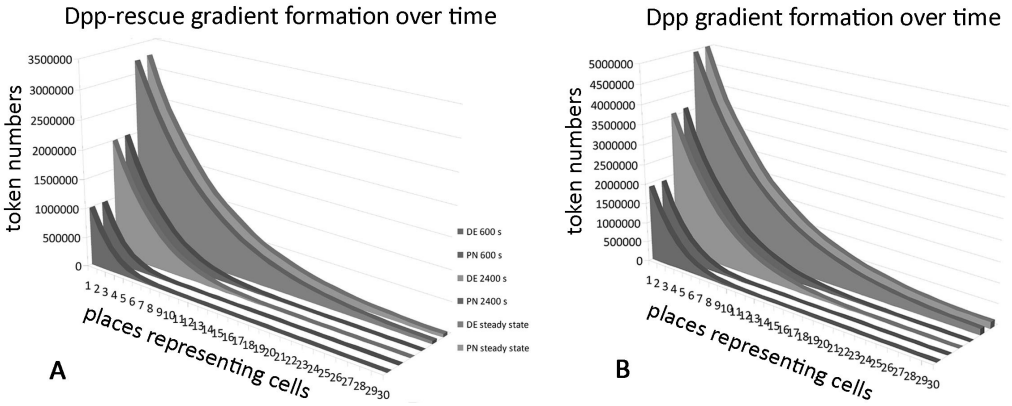

Figure 6.2. Visualisation of different states in the process of gradient formation for Dpp-rescue (A) and Dpp (B), at time points t = 600s, t =2400s and t = 12000s, of which the latter represents the steady state of the process. For each of the time points the token numbers in the places representing cells, *i.e.* x_1 to x_{30}, as predicted by the Petri net model (PN) is compared to the token numbers derived from the concentration levels, predicted by the DE model.

In addition to the steady state, we also compared the gradient formation at moments during the process, t = 600s and t = 2400s. For the DE model, these time-dependent solutions were computed using COMSOL Multiphysics package (version 4.2.0.150) for the finite element. Again the Petri net and the DE model yielded corresponding results, with minor deviations: on average 0.01% for Dpp with a maximum deviation of 0.46% and on average 0.02% for Dpp-rescue with a maximum of 0.2%. In Fig. 6.2 the Petri net marking corresponding to times t = 600s, t = 2400s and the t = 12000 are compared to those predicted by the DE model; the situation at t = 12000s represents the steady state.

6.5 CONCLUSION AND DISCUSSION

We have presented a generic Petri net model for biological gradient formation, based on the model presented in chapter 5. The current model incorporates elements from a discretised DE model for gradient formation. The resulting parametrized Petri net is more versatile and can be fitted to a wide range of instances of the process. This has been shown for the case study of Dpp and Dpp-rescue gradient formation in the fruit fly.

As with DE models, the Petri net allows quantitative analysis of gradient formation. Due to its modular nature the Petri net can easily be adjusted to other observed instances of gradient formation, both with regard to changes in parameter values and to the length of the tissue under study. While the current model represents

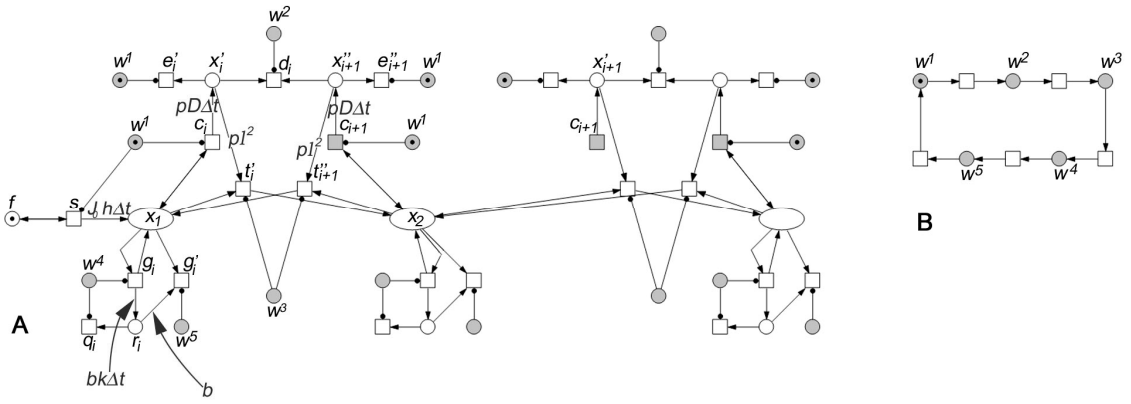

Figure 6.3. The main construction (A) of the net and auxiliary net (B) for the situation of two-directional gradient formation. Note that the main construction shown here differs from the main construction in Fig. 6.1 solely in the addition of transition t''_{i+1}.

the tissue as a one-dimensional structure, *i.e.* a line of cells, the approach is amenable to extension in two and three dimensions, by connecting cells not only in the x-dimension, but also in y- and z-dimensions. In this way the approach increases possibilities for quantitative analysis of a wide range of experimental conditions. Furthermore, by adding one transition, the Petri net can be made to model transport of tokens between neighbouring cells in two directions, as illustrated in Fig. 6.3.

The graphical element of the Petri net framework makes the process insightful to biologists and amenable to experimental setups which interfere with the unfolding of the process. In this way it becomes possible to simulate *e.g.* grafting experiments, in which part of the tissue is removed or replaced and the effects are studied. For gradient formation in particular, experiments have been performed with FRAP assays (Kicheva *et al.*, 2007; Carrero *et al.*, 2003). In these experiments part of a tissue containing fluorescently labelled proteins is locally photobleached, after which recovery of the gradient of fluorescent molecules is studied. Since the structure of the presented Petri net closely resembles the observed biological situation, it can be used to simulate similar experiments using quantitative data, by removing places which correspond to particular biological cells or depleting these of tokens.

Finally, we hope to explore possibilities of building hierarchical nets, using *e.g.* nets-within-nets (Valk, 2004) and/or refinement, to model particular subcellular processes, such as passive and active diffusion through the extracellular space and degradation by means of endocytosis, *cf.* 5.3.1.

The Petri net of gradient formation illustrates an approach that brings together aspects from process and equation based modelling techniques, *i.e.* from Petri nets and

differential equation models; this merger of techniques provides new prospects for simulation and analysis of the process of gradient formation. On a broader scale it underlines the importance of integrative methods for the field of developmental biology, which will be addressed in more detail in the next chapter.